IEEE Photonics Journal
An IEEE Photonics Society Publication

Open Access

Improving the Laser Performance of Yb^{3+}-Doped Phosphate Fiber: Population Simulation of the Yb^{3+} Level

Volume 13, Number 3, June 2021

Sasa Yan
Ying Du
Yiting Tao
Lei Zhang
Suya Feng
Danping Chen
Liyan Zhang

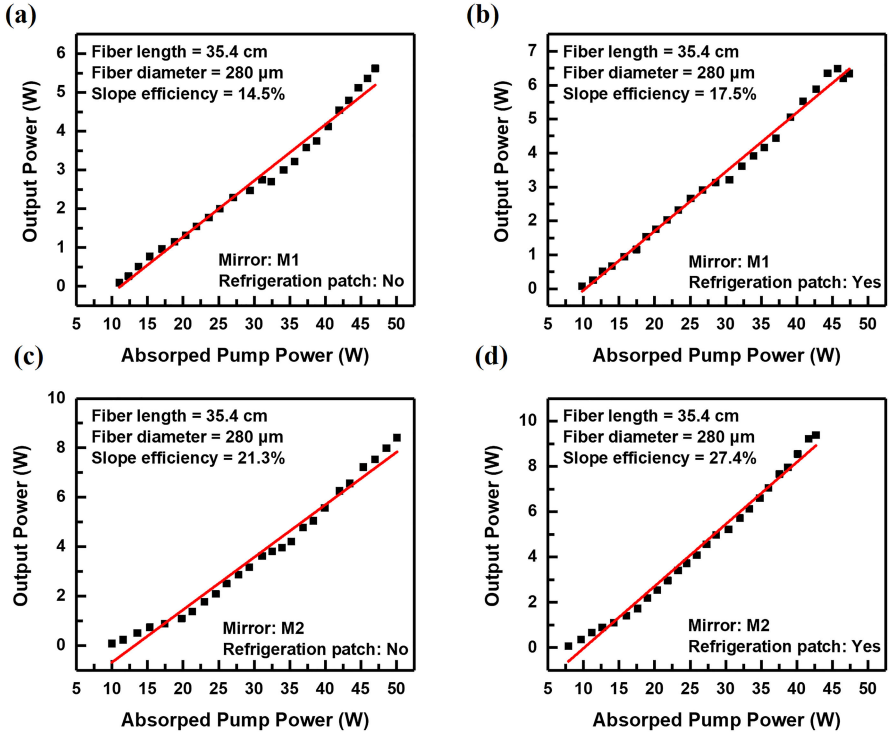

DOI: 10.1109/JPHOT.2021.3078580

Improving the Laser Performance of Yb^{3+}-Doped Phosphate Fiber: Population Simulation of the Yb^{3+} Level

Sasa Yan,[1,2] Ying Du,[1,2] Yiting Tao,[1,2] Lei Zhang,[1] Suya Feng,[1] Danping Chen,[1] and Liyan Zhang[1]

[1]Key Laboratory of Materials for High Power Laser, Shanghai Institute of Optics and Fine Mechanics, Chinese Academy of Sciences, Shanghai 201800, China
[2]Center of Materials Science and Optoelectronics Engineering, University of Chinese Academy of Sciences, Beijing 100049, China

DOI:10.1109/JPHOT.2021.3078580
This work is licensed under a Creative Commons Attribution 4.0 License. For more information, see https://creativecommons.org/licenses/by/4.0/

Manuscript received March 22, 2021; revised May 3, 2021; accepted May 5, 2021. Date of publication May 10, 2021; date of current version May 26, 2021. This work was supported by the National Natural Science Foundation of China under Grant 51872308. Corresponding authors: Danping Chen; Liyan Zhang (e-mail: d-chen@mail.siom.ac.cn; jndxzly@hotmail.com).

Abstract: Based on the Boltzmann distribution and multi-phonon relaxation probability criterion, an original Yb^{3+} population equation was proposed to describe the population distribution before and after laser generation, and the population distribution of Yb^{3+} under different pump ratios and temperatures was investigated by numerical simulation. The simulation results indicated that the laser wavelength of Yb^{3+}-doped modified phosphate fibers have a high probability of being in the range of 1019 nm–1056 nm under the conventional pump ratio. Additionally, fibers lasing at a longer wavelength may have a lower laser threshold. For ultra-high pump ratio or high fiber temperature, the laser operation state changes from a quasi-four-level to a quasi-three-level scheme, and the laser wavelength may blue-shift. Experimental results verify the above simulation results, and in addition demonstrate an output power of 9.38 W with a slop efficiency of 27.4% in an Yb^{3+}-doped phosphate modified fiber with a length of 35.4 cm and diameter of 280 μm from an optical path with a refrigeration patch and suppressing short-wave laser output. The results show that the laser performance of Yb^{3+}-doped fibers can be improved by reducing the operating temperature and inhibiting short-wave laser output.

Index Terms: Yb^{3+}-doped phosphate fiber, numerical simulation, Boltzmann distribution, Multi-phonon relaxation probability criterion.

1. Introduction

With developing semiconductor lasers, ytterbium (Yb^{3+}) is the most suitable ion of luminescent active ions for high power laser because of its small quantum defect and simple energy level [1]–[6]. Due to the high solubility of Yb^{3+} in phosphate glass [7], it is expected that it will be used in high-gain, short-length solid-state systems, such as single frequency lasers [8]–[11]. However, the narrow Stark splitting of the Yb^{3+}: $^2F_{7/2}$ level leads to a serious thermal blocking effect in solid-state Yb: phosphate glass lasers [12]. Thus, it is difficult to obtain laser output from Yb^{3+}-doped phosphate glass [13], and only 2.7 W laser output can be obtained in Yb^{3+}-doped phosphate fiber [14]. The common way is to modify the phosphate glass network, changing the field strength and symmetry of Yb^{3+}, and enhance the Stark splitting of Yb^{3+}: $^2F_{7/2}$ level, such as adding F-ion (Stark

TABLE 1
Composition of G0, G1, and G2 Glasses

Composition（mol%）	G0	G1	G2
P_2O_5	55.8	53.5	58.0
K_2O	14.9	14.3	13.5
Na_2O	4.6	4.5	2.9
BaO	9.3	8.9	9.7
Al_2O_3	5.5	5.4	5.8
Sb_2O_3	0.5	1.3	0.5
La_2O_3	0.5	0.9	0.5
Nb_2O_5	1.0	1.8	1.0
Y_2O_3	1.0	1.3	1.0
GeO_2	2.4	8.1	7.2
Pb_3O_4	1.4	-	-
Yb_2O_3	3.1	-	-

splitting from 589 cm^{-1} to 716 cm^{-1}) [15], alkaline earth metal oxides (Stark splitting from 499 cm^{-1} to 589 cm^{-1}) [16], SiO_2 (Stark splitting from 605 cm^{-1} to 808 cm^{-1}) [17], and GeO_2 (Stark splitting from 627 cm^{-1} to 815 cm^{-1}) [13], so as to improve the performance of lasing material. C. Wang *et al.* obtained an output power of 6.4 W in a GeO_2 modified Yb^{3+}-doped phosphate double-clad fiber [14], which is very close to our fiber in fiber composition and laser experiment. In fact, from the perspective of optical power density, there is no essential difference between the optical fiber studied in this paper and C. Wang's.

For a laser system, the necessary components include a laser gain medium, stable resonator, and pump source. Since a lot of research has been done to improve the laser performance by improving the properties of the material itself, here the resonator cavity and pump source are selected to explore the change in laser performance. However, whether the cavity or the pump source is changed, in essence, the laser wavelength, namely, the two sublevels chosen to produce population inversion are changed. In a steady state, the population distribution is subject to the Boltzmann distribution, whereas in the transient state, the population distribution is related to the pumping ratio and nonradiative transition. Therefore, the simulation of the Yb^{3+} population distribution under different pump ratios provides new insights for improving laser performance.

Based on the Boltzmann distribution and multi-phonon relaxation probability criterion, the relationship between the population distribution of Yb^{3+}, pump ratios, and temperature was investigated by numerical simulation. Furthermore, the simulated results were verified by changing the resonator and the use of an additional refrigeration patch in an optimized Yb^{3+}-doped phosphate fiber, which aim is to determine some methods to improve the laser performance of Yb^{3+}-doped phosphate fibers.

2. Experiment

The composition and properties of the core, inner cladding, and outer cladding glasses were listed in Table 1 and Table 2, respectively. The narrow Stark splitting of Yb^{3+}: $^2F_{7/2}$ leads to serious thermal blocking effect. Thus, enhancing the Stark splitting of $^2F_{7/2}$ is vital to improve the laser efficiency of Yb^{3+} ions in phosphate glass. The addition of GeO_2 and Pb_3O_4 to phosphate glass can significantly increase the crystal-field strength, which has become an effective method to increase Stark splitting. Here, the core glass (identified as G0) was modified phosphate glass optimized

TABLE 2
Properties of G0, G1, and G2 Glasses

Glass	n_d (at 1030 nm)	T_g (℃)	CTE (×10^{-7}/℃, 30-300 ℃)	T_s (℃)
G0	1.5510	435	128	490
G1	1.5497	489	122	537
G2	1.5314	487	119	537

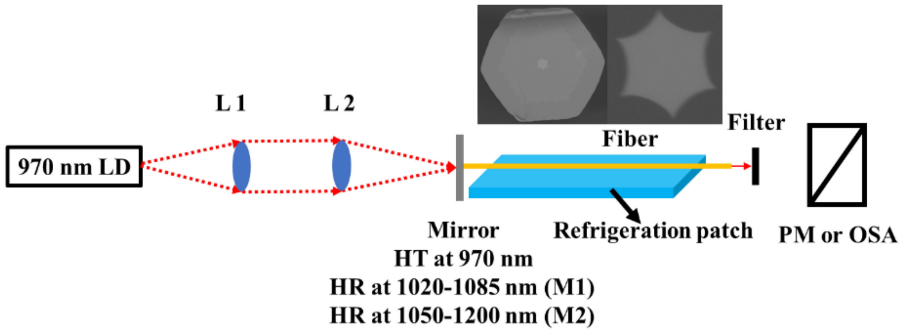

Fig. 1. Experimental device for the fiber laser test.

by GeO_2 and Pb_3O_4 doping [18], where the Yb content was approximately 10 wt%. Based on the refractive index (n_d), glass transition temperature (T_g), glass softening temperature (T_s), and expansion coefficient (*CTE*) of G0, the inner and outer cladding glasses (identified as G1 and G2, respectively) were optimized [19]. Absorption and fluorescence spectra were tested by a Lambda 950 UV/VIS/NIR spectrometer and an FLSP920 time-resolved spectrometer, respectively. Raman spectra were collected by a Renishaw inVia Raman spectrometer with 488 nm laser excitation.

The optical fiber preform was constructed by stacking small rods of G0, G1, and G2 in an inner hexagonal mold, then it was drawn into fibers with an outer diameter of ∼280 μm, inner cladding diameter of ∼190 μm, and core diameter of ∼22 μm. The loss at 1200 nm and pump absorption at 970 nm of the fiber were measured to be 2 dB/m and 20 dB/m, respectively by the cut-back method.

Fig. 1 shows the experimental device for the fiber laser test. A 970 nm laser diode (LD) was as pump source, which incident the measuring fiber through a collimating optical path consisting of L1 and L2. The dichroic mirrors (marked as M1 and M2) exhibited high transmission (HT) near 970 nm, and M1 and M2 had different wavelength range of high reflectivity (HR), which were 1020 nm–1085 nm and 1050 nm–1200 nm, respectively. A cleaved fiber end with 4.7% Fresnel reflectivity was used as a partially reflective mirror at the other end of laser cavity. A 980-nm-long pass filter was placed before the optical spectrum analyzer (OSA) or power meter (PM) to filter out the pumping source.

3. Results and Discussion

3.1 Modeling

Fig. 2 shows the absorption and fluorescence spectra of Yb^{3+}-doped G0, which were deconvoluted by Lorentzian functions. According to reference [20], the lowest Yb^{3+}: $^2F_{5/2}$ Stark splitting energy level was defined by the main absorption peak located at 974 nm, and the highest Yb^{3+}: $^2F_{7/2}$ Stark splitting energy level was determined by the longest fluorescence peak. Since this peak in phosphogermanate glasses was in the range 1050 nm–1060 nm [13], [18], the peak at ∼1056 nm was considered to be the longest fluorescence peak in G0.

Based on the deconvolution of the G0 spectra, detailed Stark splitting levels of Yb^{3+} were plotted in Fig. 3. In fact, Yb^{3+}-doped G0 tends to operate close to the quasi-four-level scheme in the optical

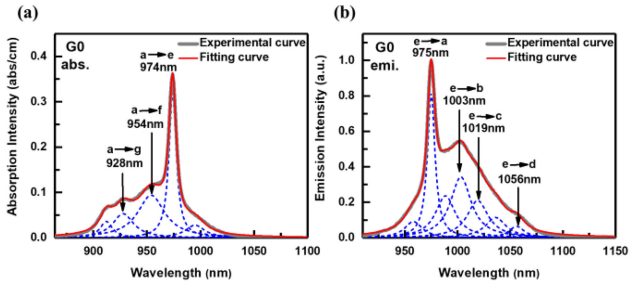

Fig. 2. Deconvolution of G0 glass spectra: (a) absorption spectrum (b) fluorescence spectrum.

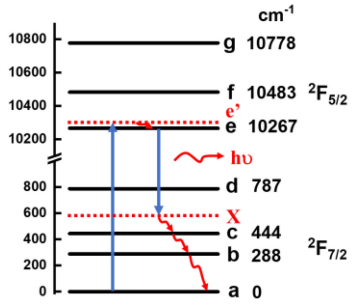

Fig. 3. Detailed Stark splitting of Yb^{3+}-doped G0.

path shown in Fig. 1. A 970 nm pump source was used to pump the population in the ground state level of $^2F_{7/2}$ ("a" level) to the "e"' level above the ground state level of $^2F_{5/2}$ ("e" level), and the energy different of "a" and "e"' levels was 10309 cm^{-1} in the G0. Due to the multi-phonon relaxation effect, the pumped population will jump to the "e" level, and moreover, there was also non-radiative transition phenomena between the $^2F_{7/2}$ levels, resulting in the redistribution of the population in these levels. Here, a specific energy level, "X," was assumed, which can be equal to the "d," "c," "b," or "a" level. When the population difference between the "X" and "e" levels reached a certain degree, a population inversion occurred, causing lasing.

The absorption and fluorescence spectra of Yb^{3+} were determined by the distributions of the populations in each Sub level "i," (i = "a," "b," "c," "d," "e," "e'," "f," "g") as shown in Fig. 3. And the temperature dependence of the population distribution of Level "i" was calculated by the Boltzmann distribution law [21].

$$\frac{N_i}{N} = \frac{e^{-\frac{E_i}{kT}}}{\sum_i e^{-\frac{E_i}{kT}}} \tag{1}$$

where N_i is the population on the Level "i" of Yb^{3+}, N is the sum of the population in all energy levels, and E_i is the energy different between the Level "i" and the bottom of the energy level, "a". T is the temperature. Furthermore, based on the Miyakawa-Dexter theory, the multi-phonon relaxation probability (W_{MPR}) between different sublevels was obtained by Eq. (2) [22].

$$W_{MPR} = Ce^{-\alpha \Delta E}\left[1 - e^{\frac{-h\omega_{\max}}{2\pi kT}}\right]^{-\frac{2\pi \Delta E}{h\omega_{\max}}} \tag{2}$$

where ΔE is the energy difference between the two sub-levels, and h and k are the Planck constant and Boltzmann constant, respectively. C and α are constants related to the base glass. According to reference [23], $C = 6.2 \times 10^7$ s^{-1} and $\alpha = 4.7 \times 10^3$ cm in phosphate base glass. $h\omega_{\max}/(2\pi)$ is the maximum phonon energy in the matrix glass and p is the required number of phonons ($p = 2\pi \Delta E/h\omega_{\max}$). In order to explore the features of Yb^{3+}-doped modified phosphate glass, the

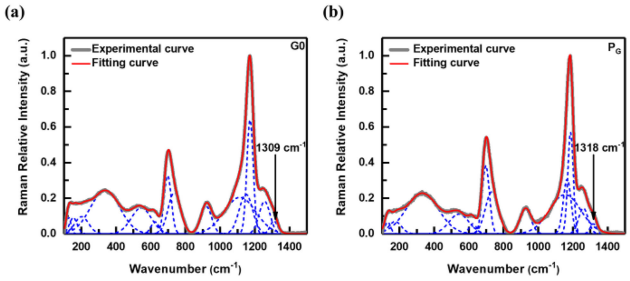

Fig. 4. Raman spectra of glasses: (a) G0; (b) P_G [18].

Yb^{3+}-doped base phosphate glass P_G was used as a reference sample [18]. As shown in Fig. 4, the maximum phonon energies of G0 and P_G were approximately 1309 cm^{-1} and 1318 cm^{-1}, respectively. For simplicity, the effect of temperature on phonon energy was ignored in the model. And based on the strong dispersion of rare earth in phosphate glass, the concentration quenching matter was also ignored in the model.

In the model, the transition between two sublevels was calculated as the product of the population of the upper level and the multi-phonon relaxation probability between the two sublevels. $W_{e'e}$, W_{dc}, W_{db}, W_{da}, W_{cb}, W_{ca}, and W_{ba} are the multi-phonon relaxation probabilities from "e'" level to "e" level, "d" to "c", "d" to "b", "d" to "a", "c" to "b", "c" level to "a", and from "b" level to "a" level, respectively. The above multi-phonon relaxation probabilities can be calculated by Eq. (2) and the energy level information in Fig. 3. In order to obtain a non-dimensional form, $W_{e'e}$, W_{dc}, W_{db}, W_{da}, W_{cb}, W_{ca}, and W_{ba} were divided by $W_{e'e}$ as $W_{e'e}{}^c$, $W_{dc}{}^c$, $W_{db}{}^c$, $W_{da}{}^c$, $W_{cb}{}^c$, $W_{ca}{}^c$, and $W_{ba}{}^c$, respectively. The initial population of Sublevels N_{i0} can be obtained from Eq. (1) and the energy level information in Fig. 3. The fluorescence area shown in Fig. 2(b) were normalized as the fluorescence branch ratio from "e" level to "d" (k_d), "c" (k_c), "b" (k_b), and "a" (k_a) level; moreover, $k_a + k_b + k_c + k_d = 1$. In the case of the lowest level "e" of $^2F_{5/2}$, the population N_e is not only the initial population on its own level (N_{e0}), but it will also receive the population from the "e'" level to "e" level through nonradiative transition ($\eta_p N_{a0} W_{e'e}{}^c$) when sample was pumped by the 970 nm LD with pumping ratio η_p, and some population [$N_f = \eta_f(N_{e0} + \eta_p N_{a0} W_{e'e}{}^c)$] will also jump to the Sublevels "d" ($k_d N_f$), "c" ($k_c N_f$), "b" ($k_b N_f$), and "a" ($k_a N_f$) with spontaneous radiation ratio η_f ($0 \leq \eta_f \leq 1$). With regard to the Sublevel "d" of $^2F_{7/2}$, the situation is a little more complicated, which population N_d originate the initial population on its own level (N_{d0}), the spontaneous radiation $k_d N_f$, and some population will also jump to the Sublevels "c" ($N_{d0} W_{dc}{}^c$), "b" ($N_{d0} W_{db}{}^c$), "a" ($N_{d0} W_{da}{}^c$). For the Sublevel "c" of $^2F_{7/2}$, N_c derived from the initial population on its own level (N_{c0}), the spontaneous radiation $k_c N_f$, and some population from the Sublevel "d" ($N_{d0} W_{dc}{}^c$), however, some population will also jump to the Sublevels "b" ($N_{c0} W_{cb}{}^c$) and "a" ($N_{c0} W_{ca}{}^c$). In the case of "b" of $^2F_{7/2}$, the population N_b mainly comes from N_{b0}, $N_{d0} W_{db}{}^c$, $N_{c0} W_{cb}{}^c$, $k_b N_f$, and some population will jump to the ground state level "a" ($N_{b0} W_{ba}{}^c$). In the same way, N_a mainly comes from N_{a0} and $N_{d0} W_{da}{}^c$, $N_{c0} W_{ca}{}^c$, $N_{b0} W_{ba}{}^c$, and $k_a N_f$, nevertheless, the difference is that some population will be pumped to the Sublevel "e'" of $^2F_{5/2}$ ($\eta_p N_{a0}$). According to Eq. (2), the multi-phonon relaxation probability between the Sublevels "e" and "d" is much smaller than that between the above sublevels, thus this scenario was ignored in the model. Thus, the population of the Sublevels "a" (N_a), "b" (N_b), "c" (N_c), "d" (N_d), and "e" (N_e) of Yb^{3+} resulting from pumping at 970 nm and η_p, and redistribution of nonradiative transition was show in Eq. (3).

$$\begin{cases} N_e = N_{e0} + \eta_p N_{a0} W_{e'e}{}^c - N_f \\ N_d = N_{d0} - N_{d0}\left(W_{dc}{}^c + W_{db}{}^c + W_{da}{}^c\right) + k_d N_f \\ N_c = N_{c0} + N_{d0} W_{dc}{}^c - N_{c0}\left(W_{cb}{}^c + W_{ca}{}^c\right) + k_c N_f \\ N_b = N_{b0} + N_{d0} W_{db}{}^c + N_{c0} W_{cb}{}^c - N_{b0} W_{ba}{}^c + k_b N_f \\ N_a = \left(1 - \eta_p\right) N_{a0} + N_{d0} W_{da}{}^c + N_{c0} W_{ca}{}^c + N_{b0} W_{ba}{}^c + k_a N_f \end{cases} \quad (3)$$

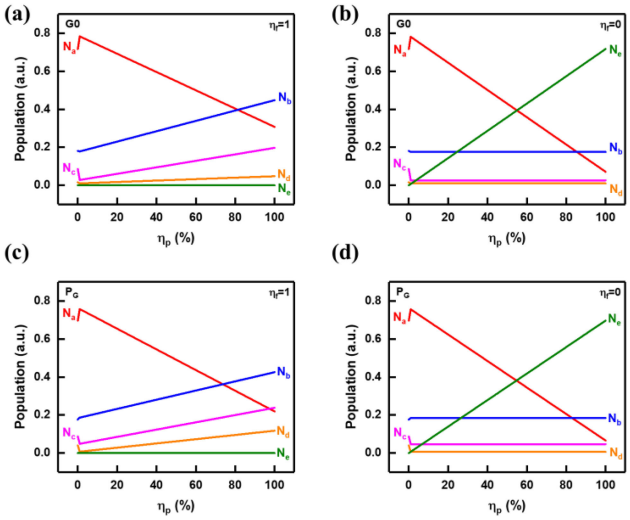

Fig. 5. Relationship between η_{p} and population distribution of Yb^{3+} sublevels at room temperature: (a) G0 glass with $\eta_f = 1$; (b) G0 glass with $\eta_f = 0$; (c) P_G glass with $\eta_f = 1$; (d) P_G glass with $\eta_f = 0$.

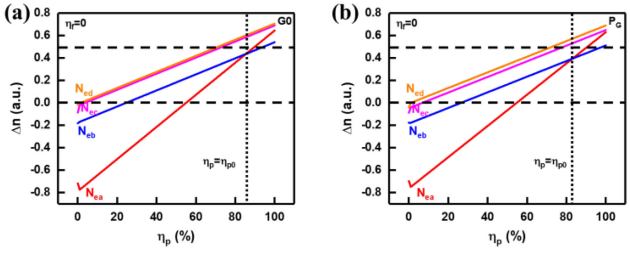

Fig. 6. Effect of η_{p} on Δn between the "e" level and the sublevels of Yb^{3+}: $^2F_{7/2}$: (a) G0; (b) P_G.

3.2 Model Solution

3.2.1 Population Distribution: Based on the data shown in Fig. 2, Eq. (3) was solved by using MATLAB R2016b software. Fig. 5 shows the influence of different pump ratios on the population of Yb^{3+} sublevels at room temperature ($T = 300$ K). Before the laser operation, almost all the upper level population fell to the lower level through spontaneous radiation according to the corresponding fluorescence branching ratios, namely $\eta_f = 1$. It can see that the population on the ground state level "a" of Yb^{3+}: $^2F_{7/2}$ obviously increased in initial period; and then rapidly reduced with increasing η_p. Moreover, the population of the Sublevel "b" increased with the increase of η_p. The population of Sublevel "c" obviously decreased in initial period; and then maintaining constant with increasing η_p. The population of Sublevel "d" increased with the increase in η_p. Especially, for the Sublevel "d" of Yb^{3+}-doped in G0 glasses, it behaved obviously decreased at the beginning. And the Sublevel "e" was almost empty with increasing η_p. When the laser was about to appear, the spontaneous radiation will be gradually suppressed due to the presence of stimulated radiation, leading to a greatly decrease in η_f. Here, for simplicity, η_f was assumed to be 0, which was used to select two sublevels that can produce population inversion. The change of "a" level was consistent with that of $\eta_f = 1$. The variation of the Sublevels "b," "c," and "d" in the initial period was similar as that of $\eta_f = 1$, and then remaining constant with increasing η_p. In addition, the population on the "e" level increased gradually with the increase of η_p.

3.2.2 Population Difference: Based on the relationship between the sublevels of Yb^{3+} and η_p in Fig. 5, the population difference (Δn) between corresponding energy levels can be calculated. The Δn between G0 and P_G glasses at different pump ratios was not compared in this paper because the Δn was a relative value obtained by specified glass. Fig. 6 describes an effect of η_p

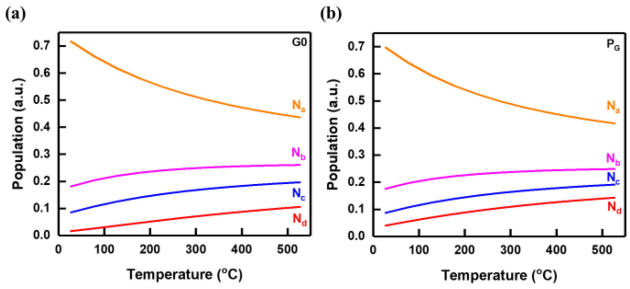

Fig. 7. Initial population distributions of Yb^{3+} sublevels at different temperatures (from room temperature to the temperature at which the glass softens): (a) the population distribution of Yb^{3+}: $^2F_{7/2}$ in G0; (b) the population distribution of Yb^{3+}: $^2F_{7/2}$ in P_G.

on Δn between the "e" level and the sublevels of Yb^{3+}: $^2F_{7/2}$. Here, N_{ea}, N_{eb}, N_{ec}, and N_{ed} are the Δn between the "e" level and "a," "b," "c," and "d" level, respectively. When $\eta_p < \eta_{p0}$, the Δn of N_{ed} and N_{ec} were clearly higher than that of N_{eb}, indicating that the probability of population inversion between the "e" level and the "d" or "c" level is higher than that between the "e" and "b" levels, implying that the laser output probability of G0 and P_G were high in the range of 1019 nm - 1056 nm and 1018 nm–1035 nm, respectively. It can also be seen that N_{ed} was higher than N_{ec}, which intimated that lasing at a longer wavelength may easily occur. The laser threshold (P_{th}) was defined as the η_p needed to achieve $\Delta n > 0$ for obtaining the laser output. When $\eta_p < \eta_{p0}$, the order of η_p needed for achieving the same Δn for each sublevel was $N_{ed} < N_{ec} < N_{eb} < N_{ea}$, namely, the sequence of P_{th} for each sublevel of Yb^{3+} was d < c < b < a. When $\eta_p > \eta_{p0}$, many populations of the "a" level were pumped to the excited state, "e'." Meanwhile, the operating state of the laser changes from the quasi-four-level to the quasi-three-level state, accompanied by intense multi-phonon relaxation in Yb^{3+}. Here the order of η_p needed for achieving the same Δn for each sublevel was $N_{ed} < N_{ec} < N_{ea} < N_{eb}$, that is to say, the sequence of P_{th} for each sublevel of Yb^{3+} was d < c < a < b. When $\eta_p = 100\%$, the population of the "a" level was almost completely pumped to the excited state, and the population inversion probability of the transition from the "e" to the "a" level increased rapidly, suggesting that the probability of the laser wavelength blue-shifting increases significantly.

3.2.3 Temperature Effect: Based on Eq. (1), the population distribution of Yb^{3+} for different temperatures can be calculated. Fig. 7 shows the initial population distribution of Yb^{3+} sublevels at different temperatures (from room temperature to softening temperature of glass). As the temperature increased, N_a decreased gradually, while the populations of the other levels increased gradually, which increased N_{ea} and decreased N_{eb}, N_{ec}, and N_{ed}. Thus, the transition probability from "e" to "a" level was increased, while the transition probability from "e" to "b," "c," or "d" level was reduced, namely, the probability of laser operation system from the quasi-four-level to the quasi-three-level laser system was increased. Here, the laser wavelength easily blue-shifted. Particularly, Δn of Yb^{3+}: $^2F_{7/2}$ in P_G was obviously smaller than that for G0, indicating that the thermal blocking effect in P_G is more serious than that of G0. In combination with the relationship between η_p and populations at each sublevel of Yb^{3+}, whether the temperature or η_p is increased, the laser operating mode changes from a quasi-four-level to a quasi-three-level laser system, and the laser wavelength easily blue-shifted.

3.3 Model Analysis

The probability of Yb^{3+} transition from the "e" level to the sublevels of $^2F_{7/2}$ can be analyzed by synthesizing the relationship between the populations and temperature, as well as the relationship between Δn and η_p. Firstly, ignore the case that "e" level transitions to "a". It will be difficult for the quasi-three-level system with high P_{th} to lase. However, when the "e" level satisfies the conditions for transition to the "a" level, population inversion between the two levels is close to that of "e"

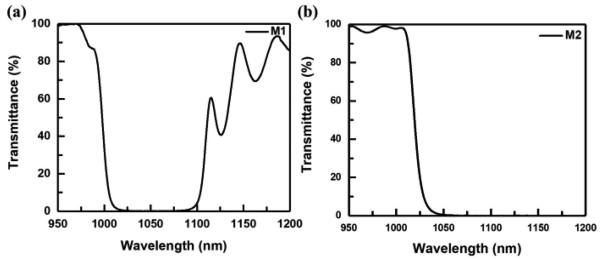

Fig. 8. Transmission spectra of mirror: (a) M1; (b) M2.

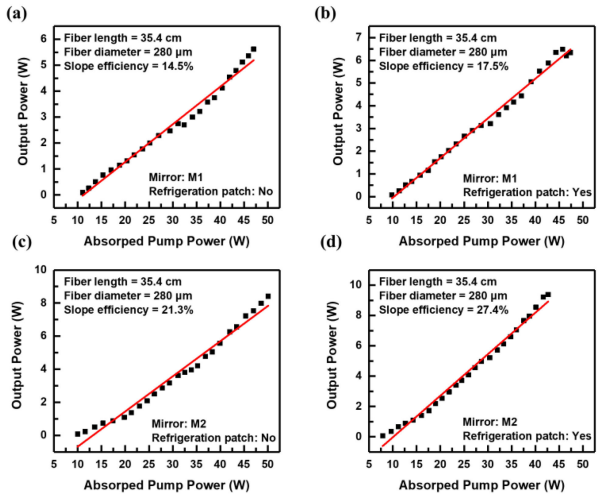

Fig. 9. Laser performance of Yb^{3+}-doped modified phosphate fiber under four conditions: (a) the optical path with M1 and without a refrigeration patch; (b) the optical path with M1 and a refrigeration patch; (c) the optical path with M2 and without a refrigeration patch; and (d) the optical path with M2 and a refrigeration patch.

jumping to the "d" or "c" level. At this time, $\eta_p > \eta_{p0}$, while the population of the "a" level are almost pumped to the excited state, leading to a large Δn between the "e" and "a" levels. Based on Eq. (2), small ΔE means large W_{MPR}. Thus, the probability of multi-phonon relaxation between the sublevels of $^2F_{7/2}$ is large because of their narrow energy level interval. In the absence of a cooling system, fiber will generate a large amount of hot, which will not only increase the thermal blocking effect, but may damage the fiber structure. Thus, to obtain high slope efficiency and low laser threshold, lasing generated by the "e" level to "d" or "c" level transitions was generally considered. In other words, the laser performance can be improved by selecting long wavelength laser output.

3.4 Model Validation

A verification experiment was performed using an Yb^{3+}-doped modified phosphate fiber (length: 35.4 cm, diameter: 280 μm) in the optical path shown in Fig. 1. The transmittance of M1 and M2 was shown in Fig. 8. Fig. 9 displays the laser performance of this fiber under four conditions. Table 3 lists the laser properties, including the laser wavelength near the laser threshold (λ_{th}), the laser threshold (P_{th}), the laser slope efficiency (η), and the maximum laser output power ($P_{\max}$). From the information provided in Fig. 7 and Table 3, two conclusions can be drawn: one was that high P_{th}, low η, and low $P_{\max}$ were obtained from the fiber without a refrigeration patch; the other was that low P_{th}, high η, and high $P_{\max}$ were obtained from the fiber with mirror suppressing the short-wave laser output. Therefore, the laser performance, including P_{th}, η, and $P_{\max}$, can be improved by reducing the fiber temperature, suppressing the short-wave output, and enhancing the

TABLE 3
Laser Properties of Yb3+-Doped Modified Phosphate Fiber Under Four Conditions

Experiment	Mirror	Refrigeration patch	λ_{th} (nm)	P_{th} (W)	η (%)	P_{max} (W)
1	M1	No	1023	11.0	14.5	5.62
2	M1	Yes	1024	9.8	17.5	6.34
3	M2	No	1029	10.0	21.3	8.41
4	M2	Yes	1029	7.9	27.4	9.38

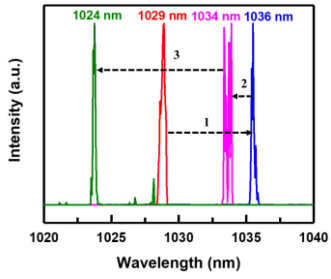

Fig. 10. Change in laser wavelength in the optical path with M2 and a refrigeration patch.

long-wave laser output probability. These conclusions are consistent with the predicted results of the model.

Fig. 10 shows the change in laser wavelength in the optical path with M2 and a refrigeration patch. Initially, the laser wavelength increased with increasing pump power (from 1029 nm to 1036 nm). However, when the pump power further increased, the laser wavelength decreased (from 1036 nm to 1024 nm). In other words, when η_{p} is low, the laser wavelength shifts toward the long-wave with increasing η_p. When η_p reaches a certain level, the laser wavelength shifts toward to the short-wave with increasing η_p. The results are similar to those predicted by the model.

3.5 Model promotion and Improvement

Due to the model assumption and the limitation of experimental conditions, the model is not perfect. And the promotion and improvement of model can be carried out from four aspects, namely introducing laser rate equation, temperature, concentration quenching factor and different pumping wavelength. Introducing the laser rate equation used for modeling, since it can clear how the graphs comparing the simulation and experimental results. Introducing temperature and discussing the thermo optic effect on fiber, especially the expansion coefficient of phosphate glass is large, which will affect many aspects, such as the refractive index. Considering the concentration quenching factor, this model can be further modified by the experimental date of ultra-high Yb^{3+}-doped phosphate fibers. Also, this model can be further verification by the pump wavelength used as 915 nm or 940 nm. And this model can be modified by the experimental results of different pumping wavelengths.

4. Conclusion

In this paper, based on the Boltzmann distribution and multi-phonon relaxation probability criterion, an original Yb^{3+} population equation was proposed to describe the population distribution before and after laser generation, and the relationship between the population distribution of Yb^{3+}, η_p, and temperature was investigated by a numerical simulation method. The simulation result indicated

that the laser wavelength of Yb^{3+}-doped modified phosphate fibers had high probability in the range of 1019 nm and 1056 nm when $\eta_p < \eta_{p0}$. The fibers with a longer laser wavelength may have a lower P_{th}. When $\eta_p > \eta_{p0}$, the laser operation state changed from a quasi-four-level to a quasi-three-level scheme and the laser wavelength shifted toward the short-wave. Moreover, the thermal blocking effect of Yb^{3+} was aggravated by the increase in temperature, and there was an easy transition from the "e" level to the "a" level, namely, from a quasi-four-level to a quasi-three-level laser system. This was accompanied by a shift toward short-wave laser output. Specifically, Yb^{3+}-doped modified phosphate glass G0 can improve the thermal blocking effect in P_G, thus greatly improving the laser performance. A verification experiment was performed using a 35.4-cm-long fiber with a diameter of 280 μm under four conditions. The experimental results validated the simulation results. Further, an output power of 9.38 W with a slope efficiency of 27.4% were obtained for this fiber from an optical path with a refrigeration patch, and short-wave laser output was suppressed. The results show that the laser performance of Yb^{3+} doped fibers can be improved by reducing the operating temperature and inhabiting short-wave laser output.

References

[1] J. Liu *et al.*, "A design of a surface-doped Yb: YAG slab laser with high power and high efficiency," *Chin. Opt. Lett.*, vol. 16, 2018, Art. no. 101401.

[2] B. A. Reagan *et al.*, "Scaling diode-pumped, high energy picosecond lasers to kilowatt average powers," *High Power Laser Sci. Eng.*, vol. 6, 2018, Art. no. e11.

[3] W. L. Tian *et al.*, "Diode-pumped power scalable Kerr-lens mode-locked Yb: CYA laser," *Photon. Res.*, vol. 6, pp. 127–131, 2018.

[4] Y. B. Wang, G. Chen, and J. Y. Li, "Development and prospect of high-power Yb^{3+} doped fibers," *High Power Laser Sci. Eng.*, vol. 6, 2018, Art. no. e40.

[5] Q. Gao, H. L. Zhang, and J. Fayyaz, "Laser diode partially end-pumped electro-optically Q-switched Yb: YAG slab laser," *Chin. Opt. Lett.*, vol. 17, 2019, Art. no. 111405.

[6] W. L. Tian *et al.*, "Sub-40-fs high-power Yb: CALYO laser pumped by single-mode fiber laser," *High Power Laser Sci. Eng.*, vol. 7, 2019, Art. no. e64.

[7] M. J. V. Bell, W. G. Quirino, S. L. Oliveira, D. F. De Sousa, and L. A. O. Nunes, "Cooperative luminescence in Yb^{3+}-doped phosphate glasses," *J. Phys. Condens. Matter*, vol. 15, pp. 4877–4887, 2003.

[8] S. H. Xu *et al.*, "400 mW ultrashort cavity low-noise single-frequency Yb^{3+}-doped phosphate fiber laser," *Opt. Lett.*, vol. 36, pp. 3708–3710, 2011.

[9] S. H. Xu *et al.*, "Low noise single-frequency single-polarization ytterbium-doped phosphate fiber laser at 1083 nm," *Opt. Lett.*, vol. 38, pp. 501–503, 2013.

[10] C. S. Yang *et al.*, "High-efficiency watt-level 1014 nm single-frequency laser based on short Yb-doped phosphate fiber amplifiers," *Appl. Phys. Exp.*, vol. 7, 2014, Art. no. 062702.

[11] C. Li *et al.*, "Experimental investigation on linewidth characteristics of a single-frequency phosphate fiber laser at 1.0 μm," *Laser Phys.*, vol. 25, 2015, Art. no. 025103.

[12] P. H. Haumesser, R. Gaume, B. Viana, E. Antic-Fidancev, and D. Vivien, "Spectroscopic and crystal-field analysis of new Yb-doped laser materials," *J. Phys. Condens. Matter*, vol. 13, pp. 5427–5447, 2001.

[13] L. Y. Zhang and H. Li, "Lasing improvement of Yb: phosphate glass with GeO_2 modification," *J. Lumin.*, vol. 192, pp. 237–242, 2017.

[14] C. Wang, Y. J. Wang, L. Y. Zhang, and D. P. Chen, "Effect of GeO_2 on the lasing performance of Yb: Phosphate glass fiber," *Opt. Mater.*, vol. 64, pp. 208–211, 2017.

[15] L. Y. Zhang, T. F. Xue, D. B. He, M. Guzik, and G. Boulon, "Influence of Stark splitting levels on the lasing performance of Yb^{3+} in phosphate and fluorophosphate glasses," *Opt. Exp.*, vol. 23, pp. 1505–1511, 2015.

[16] P. Wang, "Study of the Stark splitting of Yb^{3+} in phosphate glass," The University of Chinese Academy of Sciences, 2016.

[17] Y. J. Wang, C. Wang, S. Kang, and L. Y. Zhang, "Influence of SiO_2 on the Stark splitting and spectroscopic properties of Yb^{3+} in phosphate glass," *J. Lumin.*, vol. 186, pp. 268–272, 2017.

[18] S. S. Yan, Y. Yue, Y. J. Wang, Y. C. Diao, D. P. Chen, and L. Y. Zhang, "Effect of GeO_2 on structure and properties of Yb: Phosphate glass," *J. Non-Cryst. Solids*, vol. 520, 2019, Art. no. 119455.

[19] S. S. Yan *et al.*, "Accelerating design of matching glass for phosphate fiber cores: Multi-parameter inversion model," *Mater. Today Commun.*, vol. 25, 2020, Art. no. 101340.

[20] G. Boulon, "Why so deep research on Yb^{3+}-doped optical inorganic materials?," *J. Alloys Compounds*, vol. 451, pp. 1–11, 2008.

[21] D. A. Grukh, A. S. Kurkov, V. M. Paramonov, and E. M. Dianov, "Effect of heating on the optical properties of Yb^{3+}-doped fibres and fibre lasers," *Quantum Electron.*, vol. 34, pp. 579–582, 2004.

[22] C. B. Layne, W. H. Lowdermilk, and M. J. Weber, "Multiphonon relaxation of rare-earth ions in oxide glasses," *Phys. Rev. B*, vol. 16, pp. 10–20, 1977.

[23] J. M. F. Vandijk and M. F. H. Schuurmans, "On the nonradiative and radiative decay rates and a modified exponential energy gap law for 4f–4f transitions in rare-earth ions," *J. Chem. Phys.*, vol. 78, pp. 5317–5323, 1983.